Optics Communications 334 (2015) 94–100

Contents lists available at ScienceDirect

Optics Communications

journal homepage: www.elsevier.com/locate/optcom

Cavity linewidth narrowing by tunneling induced double dark resonances in triple quantum dot molecules

Si-Cong Tian [a], Ren-Gang Wan [b], Lian-He Li [a], Cun-Zhu Tong [a,*], Yong-Qiang Ning [a]

[a] State Key laboratory of Luminescence and Applications, Changchun Institute of Optics, Fine Mechanics and Physics, Chinese Academy of Sciences, Changchun 130033, China

[b] State Key Laboratory of Transient Optics and Photonics, Xi'an Institute of Optics and Precision Mechanics, Chinese Academy of Sciences, Xi'an 710119, China

ARTICLE INFO

Article history:
Received 5 June 2014
Received in revised form
25 July 2014
Accepted 4 August 2014
Available online 15 August 2014

Keywords:
Triple quantum dots
Electromagnetically induced transparency
Cavity transmission spectrum
Linewidth narrowing

ABSTRACT

A scheme for obtaining a tunable ultranarrow cavity transmission controlled by two tunneling in triple quantum dots system is proposed. In such system, the tunneling can induce double dark resonances, resulting in the appearance of two transparency windows. With the steep dispersion within the narrowed transparency windows, an ultranarrow transmission peak can be obtained, compared with that of double quantum dots system. Furthermore, by varying the energy splitting, the linewidth and the position of the ultranarrow transmission peak can be engineered. Because no coupling laser is required, the scheme proposed here is more convenient for future experiments and applications in optics, and may be useful in designing novel optoelectronic devices.

1. Introduction

The phenomenon of electromagnetically induced transparency (EIT) plays an important role in the interaction between light and matter because EIT has found numerous applications [1,2]. Reduced absorption and high dispersion produced by EIT can induce cavity-linewidth narrowing, which is known as intracavity EIT termed by Lukin et al. [3]. Cavity-linewidth narrowing was experimentally first observed in hot atomic vapor [4], then in a cold atomic system [5] and in a Doppler broadened medium [6]. On the other hand, dark resonance is the basic of EIT. When a dark state is coherently coupled to another level by a coupling laser, double dark resonances can be acquired, which is first predicted by Lukin et al. [7] and later experimentally observed by Chen et al. [8]. With the aid of the double dark resonances, the optical responses of atoms can be well manipulated [9–12], many works such as nonlinearity optics [9,10], atom localization [11], optical bistability [12] are studied.

The above works are carried out in atomic medium and coupling lasers are necessary in such systems. On the other hand, semiconductor quantum dots (QDs) have the similar property to those of atoms, owing to the confinement of electrons and holes, which encouraged us to extend the above studies to QDs. Furthermore, two or more quantum dots coupled by tunneling can form quantum dot molecules (QDMs), in which the tunneling of electrons or holes can be controlled by an external electric field and create a multilevel structure of excitonic states. Experimentally, double quantum dots (DQDs) have been realized in both vertical [13] and lateral [14] type, and have been used for optical spectroscopy [15], excitonic entanglement [16], single photon and spin storage [17], and coherent population trapping (CPT) [18]. On the theoretical side, many works have been carried out about DQDs, such as EIT and slow light [19–21], entanglement [22–25], optical bistability [26,27], coherent population transfer [28], narrowing of transmission spectrum [29] and fluorescence spectrum [30].

Building on DQDs with controlled electron numbers, triple quantum dots (TQDs) have also been achieved in much experimental progress [31–34]. Most recently, transmission-dispersion characteristics of waveguide-coupled photonic crystal two-mode nanocavity embedding TQDs have been studied [35]. And it is also proposed to simulate spontaneously generated coherence (SGC) in TQDs [36]. And giant Kerr nonlinearity can also been achieved in TQDs [37]. In this paper, we propose a scheme for obtaining a tunable ultranarrow cavity transmission in TQDs. Our work is mainly based on [3–6,29,38–40], however, the scheme proposed here is very different from those. First, in TQDs two tunneling couplings can induce double dark resonances, resulting in two transparency windows. And close to the narrowed transparency window, a tunable ultranarrow cavity transmission can be obtained. Such results can not be obtained in usual three-level

* Corresponding author.
E-mail addresses: tiansicong@ciomp.ac.cn (S.-C. Tian), tongcz@ciomp.ac.cn (C.-Z. Tong).

http://dx.doi.org/10.1016/j.optcom.2014.08.011
0030-4018/

atomic [3–6] or DQDs [29] systems. Second, an important advantage of our scheme is that we use tunneling instead of coupling lasers [38–40] to obtain cavity-linewidth narrowing, which can be controlled by the external electric field. Therefore the scheme proposed here is more convenient for experiments and applications in optics.

The paper is organized as follows: in Section 2, we introduce the model and the basic equations. In Section 3, we plot the absorption and dispersion spectrum. In Section 4, we plot the transmission spectrum. Section 5 is the conclusions.

2. Models and equations

We show the schematic of the setup, the band structure and level configuration of TQDs system in Fig. 1. At nanoscale interdot separation, the hole states are localized in the QDs and the electron states are rather delocalized. In TQDs system, the tunneling can be controlled by placing a gate electrode between the neighboring dots. In the absence of a gate voltage, the conduction-band electron levels are out of resonance and the electron tunneling between the QDs is very weak. In contrast, in the presence of a gate voltage, the conduction-band electron levels come close to resonance and the electron tunneling between the QDs is greatly enhanced. And in the latter case the hole tunneling can be neglected because of the more off-resonant valence-band energy levels. Therefore we can give the schematic of the level configuration of TQDs, as shown in Fig. 1(c). Without the excitation of the laser, no excitons are inside all QDs, which corresponds to state $|0\rangle$. When a laser field is applied, a direct exciton is created inside the QD1, condition represented by the state $|1\rangle$. Under the tunneling couplings, the electron can tunnel from QD1 to the QD2, and from QD2 to QD3. And we denote these indirect excitons as state $|2\rangle$ and state $|3\rangle$, respectively.

Under the rotating-wave and the electric-dipole approximations, and after performing the unitary transformation $U = e^{-i\omega_p t}(|1\rangle\langle 1| + |2\rangle\langle 2| + |3\rangle\langle 3|)$, which removes the time-dependent oscillatory terms, the Hamiltonian under the basis $\{|0\rangle, |1\rangle, |2\rangle, |3\rangle\}$ can be written as (assumption of $\hbar = 1$)

$$H_I = \begin{pmatrix} 0 & -\Omega_p & 0 & 0 \\ -\Omega_p & \delta_p & -T_1 & 0 \\ 0 & -T_1 & \delta_p - \omega_{12} & -T_2 \\ 0 & 0 & -T_2 & \delta_p - \omega_{12} - \omega_{23} \end{pmatrix}. \tag{1}$$

Here $\Omega_p = \boldsymbol{\mu}_{10} \cdot \mathbf{e} \cdot E_p$ is the Rabi frequency of the transition $|0\rangle \to |1\rangle$, with $\boldsymbol{\mu}_{10}$ being the associated dipole transition-matrix element, $\mathbf{e}$ the polarization vector and E_p the electric-field amplitude of the probe laser. And T_1 and T_2 are the tunneling couplings, which depend on the barrier characteristics and the external electric field. $\delta_p = \omega_{10} - \omega_p$ is the detuning of the probe field, with ω_p being the frequency of the probe field and ω_{10} being the transition frequency between $|1\rangle$ and $|0\rangle$ states. ω_{12} and ω_{23} are the energy splitting of state $|1\rangle$ and $|2\rangle$, and state $|2\rangle$ and $|3\rangle$, respectively. Experimentally, ω_{12} and ω_{23} can be changed by

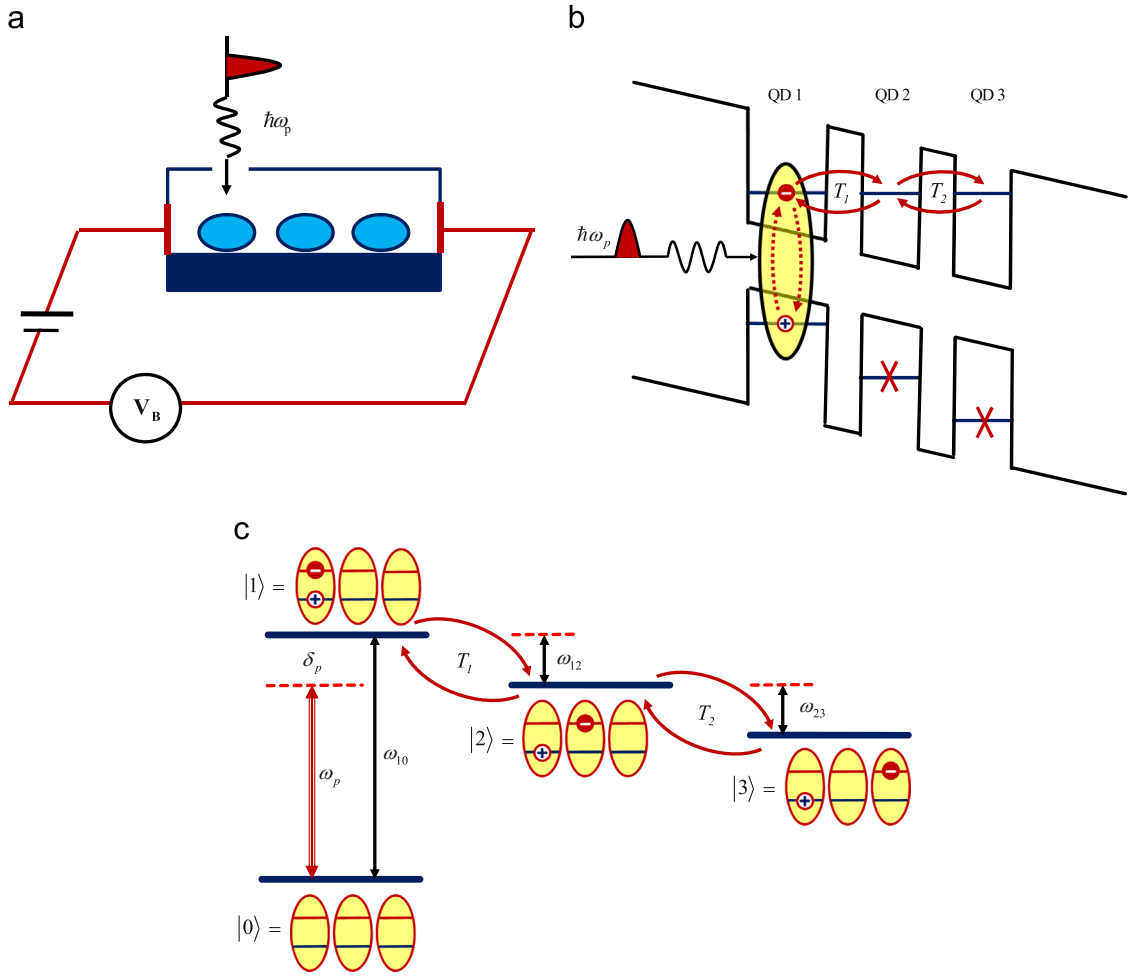

Fig. 1. (a) The schematic of the setup of TQDs. The probe field transmits the QD 1. V_B is a bias voltage. (b) The schematic of the band structure of TQDs. (c) The schematic of the level configuration of TQDs.

manipulation of the external electric field that changes the effective confinement potential.

At any time t, the state vector can be written as

$$|\Psi_I(t)\rangle = a_0(t)|0\rangle + a_1(t)|1\rangle + a_2(t)|2\rangle + a_3(t)|3\rangle. \quad (2)$$

The evolution of the state vector obeys the Schrödinger equation

$$\frac{d}{dt}|\Psi_I(t)\rangle = -iH_I(t)|\Psi_I(t)\rangle. \quad (3)$$

Substituting Eq. (1) and Eq. (2) into Eq. (3), and then using the Weisskopf–Wigner theory [41,42], we can obtain the following dynamical equations for atomic probability amplitudes in the interaction picture:

$$i\dot{a}_0 = -\Omega_p a_1, \quad (4a)$$

$$i\dot{a}_1 = -\Omega_p a_0 - T_1 a_2 + (\delta_p - i\gamma_1)a_1, \quad (4b)$$

$$i\dot{a}_2 = -T_1 a_1 - T_2 a_3 + (\delta_p - \omega_{12} - i\gamma_2)a_2, \quad (4c)$$

$$i\dot{a}_3 = -T_2 a_2 + (\delta_p - \omega_{12} - \omega_{23} - i\gamma_3)a_3, \quad (4d)$$

$$|a_0|^2 + |a_1|^2 + |a_2|^2 + |a_3|^2 = 1, \quad (4e)$$

where $\gamma_i = \frac{1}{2}\Gamma_{i0} + \gamma_{i0}{}^d (i = 1-3)$ is the typical effective decay rate, with Γ_{i0} being the radiative decay rate of populations from $|i\rangle \to |0\rangle$ and $\gamma_{i0}{}^d$ being the pure dephasing rates.

In the limit of a weak probe signal, almost all excitons will remain in state $|0\rangle$ and hence we may assume that $|a_0\rangle \cong 1$. Under this assumption, we can solve Eq. (4) for the steady-state values of the probability amplitudes, from which one arrives at the following probe susceptibility

$$\chi(\delta_p) = \frac{N|\boldsymbol{\mu}_{10}|^2}{\varepsilon_0 \hbar} \frac{1}{\Gamma_1 - \frac{T_1{}^2 \Gamma_3}{\Gamma_2 \Gamma_3 - T_2{}^2}}, \quad (5)$$

with $\Gamma_1 = \delta_p - i\gamma_1$, $\Gamma_2 = \delta_p - \omega_{12} - i\gamma_2$, $\Gamma_3 = \delta_p - \omega_{12} - \omega_{23} - i\gamma_3$. And $N = (\Gamma/V)$ is the excitons volume density, with Γ being the optical confinement factor, V being the volume of the TQDs, ε_0 is the dielectric constant, and $\boldsymbol{\mu}_{10}$ is the associated dipole transition-matrix element [43].

And for simplicity, we set the absorption cross-section as [44,45]

$$\sigma_{10} = \frac{\omega_{10}}{c} \frac{|\boldsymbol{\mu}_{10}|^2}{\varepsilon_0 \hbar \gamma_1}, \quad (6)$$

where c is the velocity of the light in vacuum. Thus Eq. (5) can be written as

$$\chi(\delta_p) = N\gamma_1 \frac{c}{\omega_{10}} \sigma_{10} \frac{1}{\Gamma_1 - \frac{T_1{}^2 \Gamma_3}{\Gamma_2 \Gamma_3 - T_2{}^2}}. \quad (7)$$

The susceptibility χ can be separated into real (χ') and imaginary (χ'') parts, which represent the absorption and dispersion of the medium, respectively.

3. Absorption and dispersion spectrum of TQDs

In this part we plot in Fig. 2 the absorption (χ'') and dispersion (χ') spectrum according to Eq. (7) for different parameters. We point out that the absorption and dispersion spectrum have been studied in an atomic system with the coupling lasers [7,8]. But here we use tunneling instead of the coupling lasers and obtain similar results.

In TQDs, the tunneling coupling T_1 and T_2 depend on the barrier characteristics and the external electric field. Energy splitting ω_{12} and ω_{23} can be done by manipulation of the external electric field that changes the effective confinement potential. In addition, in this investigation we work in the low temperature regime, and consider both the population decay rates and the dephasing rates. The realistic values of the parameters are according to Ref. [20] and Refs. therein [46–53]. And for simplicity, all the parameters are scaled by the decay rate γ_1. Though some of the value of parameters are for DQDs, it can be inferred that the tunneling, energy splitting and decay rates of TQDs have the same values with that of DQDs.

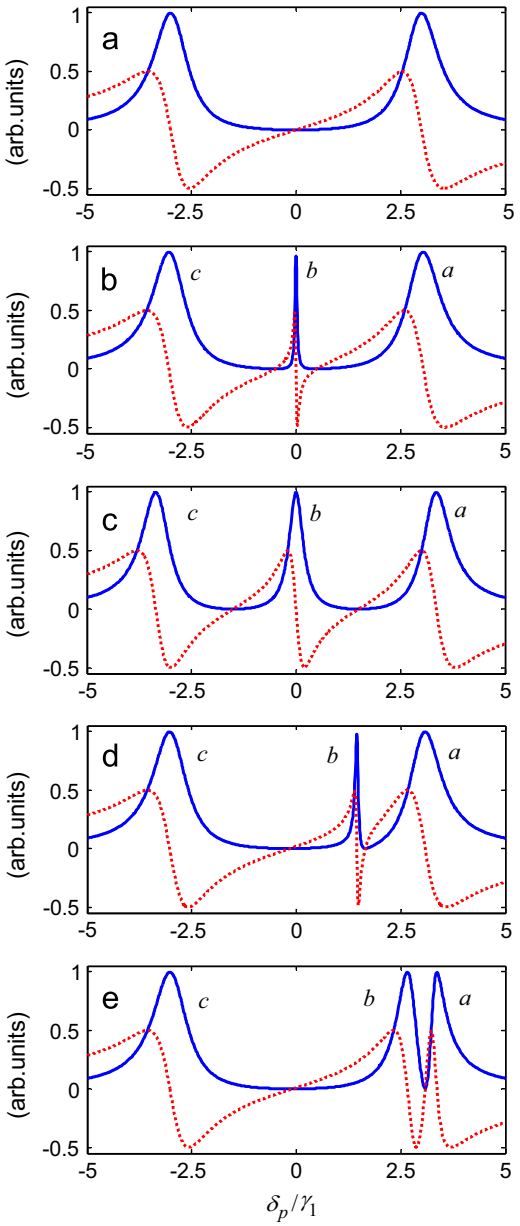

Fig. 2. The absorption spectrum (solid line) and dispersion spectrum (dotted line) as a function of δ_p. The parameters are (a) $T_1 = 3$, $T_2 = 0$, $\omega_{12} = \omega_{23} = 0$, (b) $T_1 = 3$, $T_2 = 0.5$, $\omega_{12} = \omega_{23} = 0$, (c) $T_1 = 3$, $T_2 = 1.5$, $\omega_{12} = \omega_{23} = 0$, (d) $T_1 = 3$, $T_2 = 0.5$, $\omega_{12} = 0$, $\omega_{23} = 1.5$, and (e) $T_1 = 3$, $T_2 = 0.5$, $\omega_{12} = 0$, $\omega_{23} = 3$. Other parameters are $\gamma_1 = 1$, $\gamma_2 = \gamma_3 = 10^{-3}\gamma_1$. And all the parameters are scaled by γ_1. The three absorption peaks are numbered with *a*, *b* and *c*.

First, we short the third QD from the system, which means that only the tunneling T_1 couples to the system. Therefore the electron can only transfer from QD1 to QD2, creating three-level Λ system. And in such case, with $\omega_{12} = 0$, one can obtain two absorption peaks and one transparency window in the absorption spectrum. And within the transparency window, a dispersion spectrum similar to DQDs shows up (Fig. 2(a)). Once the two tunneling couplings are applied to the system, the electron can tunnel from

QD 1 to QD 2 and then from QD 2 to QD 3, which forms TQDs. In this case, one extra absorption peak appears in the middle of the absorption spectrum and the transparency window splits into two transparency windows. We show these situations for $\omega_{12}=\omega_{23}=0$ in Fig. 2(b) and (c), and find that with the larger value of the tunneling T_2, the two transparency windows become further away from each other, but the linewidth of these two transparency windows are nearly unchanged. And within the two transparency windows, the slope of the dispersion is the same, due to the symmetrical absorption spectrum. Next we show the case of $\omega_{23}\neq 0$ in Fig. 2(d) and (e). One can see that the absorption spectrum becomes unsymmetrical, with one transparency window being much narrower than the other. As the value of ω_{23} is increasing, the right transparency window moves farther away from the center of the spectrum, and the width of this transparency window is becoming narrower.

So it can be concluded that the tunneling coupling T_2 and the energy splitting ω_{23} of TQDs can modify the position and the width of the transparency windows. And with larger value of ω_{23}, the width of the transparency window becomes narrower. In the area of the narrower transparency window, much larger dispersion can be obtained.

In the following part we will give a short expansion for the above results. First we explain the emersion of two transparency windows and the controlling of the position of these transparency windows. With only one tunneling coupling T_1, the system is similar to a DQDs and the appearance of the transparency window is owning to the dark state induced by the tunneling T_1, which can been written as $|\Psi_{Dark}\rangle=\frac{1}{\sqrt{\Omega_p^2+T_1^2}}(T_1|0\rangle-\Omega_p|2\rangle)$ under the resonant coupling. And when tunneling T_2 is also applied to the system, this extra tunneling can make state $|2\rangle$ split into two dressed levels $|2_\pm\rangle$ with splitting of $\sqrt{4{T_2}^2+{\omega_{23}}^2}$, therefore two Λ type subsystems can be created, as shown in Fig. 3(a). In such two Λ type subsystems, the existence of two distinct dark states $|\Psi_{Dark\pm}\rangle=\frac{1}{\sqrt{\Omega_p^2+T_{1\pm}^2}}(T_{1\pm}|0\rangle-\Omega_p|2_\pm\rangle)$ is clear, where $T_{1\pm}$ denote the tunneling couplings between the state $|1\rangle$ and $|2_\pm\rangle$. And each dark state corresponds to a two-photon resonance between the state $|0\rangle$ and $|2_\pm\rangle$, and the state $|0\rangle$ and $|2_-\rangle$, respectively. Therefore the single transparency window splits into two transparency windows, which are located at the position of $\delta_p=\frac{\omega_{23}\pm\sqrt{{\omega_{23}}^2+{T_2}^2}}{2}$ (for $\omega_{12}=0$). Therefore the position of the transparency windows is determined by the value of T_2 and ω_{23}.

To understand the narrowing of the transparency window, we consider the fully dressed state picture for both tunneling couplings. In this way state $|1\rangle$, $|2\rangle$ and $|3\rangle$ in the bare state can be replaced by three new dressed states $|a\rangle$, $|b\rangle$ and $|c\rangle$, and these dressed states decay to the ground state $|0\rangle$ with decay rate γ_a, γ_b and γ_c, respectively. And the expression of the dressed states and the corresponding decay rates can be written as

$$|i\rangle=\cos\varphi\cos\theta|1\rangle+\sin\varphi|2\rangle+\cos\varphi\sin\theta|3\rangle,(i=a,b,c) \tag{8a}$$

$$\gamma_i=\cos^2\varphi\cos^2\theta\gamma_1+\sin^2\varphi\gamma_2+\cos^2\varphi\sin^2\theta\gamma_3,\ (i=a,b,c) \tag{8b}$$

where $\tan\varphi=AB/\sqrt{A^2+B^2}$, $\tan\theta=A/B$, $A=\lambda_i/T_1$ and $B=(\lambda_i-\omega_{12}-\omega_{23})/T_2$. And λ_i is the eigenvalues of the dressed level $|i\rangle$, giving the relative energy of the dressed sublevels $|i\rangle$. We show the schematic diagram of the dressed states in Fig. 3(b), the weak probe field couples the transition from state $|0\rangle$ to the dressed state $|i\rangle$, and the decay rate from $|i\rangle$ to the ground state is $\gamma_i(i=a,b,c)$. If the frequency of the probe field is chosen such that it is in resonance with one of the transition $|0\rangle\leftrightarrow|i\rangle$, then the maximal absorption is obtained. Therefore the position of the absorption peaks is determined by the eigenvalues $\lambda_i(i=a,b,c)$, and the width of the absorption peaks is determined by the decay rates $\gamma_i(i=a,b,c)$. (In Fig. 2 we number the three absorption peaks with a, b and c, which comes from the corresponding transition $|0\rangle\leftrightarrow|i\rangle$.) And the destructive interference between the three absorptive channels $|0\rangle\rightarrow|a\rangle$ and $|0\rangle\rightarrow|b\rangle$, also $|b\rangle\leftrightarrow|0\rangle$ and $|0\rangle\rightarrow|c\rangle$ can result to two transparency windows, which locate between these three absorption peaks. And the width of the transparency windows depend on the linewidth and the position of the absorption peaks. The wide linewidth and close spaced of the absorption peaks will result in the narrow transparency windows.

We show in Fig. 4(a) the eigen energies $(\lambda_i, i=a,b,c)$ and in Fig. 4(c) the decay rates $\gamma_i(i=a,b,c)$ as a function of T_2, and in Fig. 4(b) the the eigen energies $(\lambda_i, i=a,b,c)$ and in Fig. 4(d) the decay rates $\gamma_i(i=a,b,c)$as a function of ω_{23}, respectively. From Fig. 4(a), one can see that for all values of T_2, the energy difference of the three dressed states are large, therefore the three absorption peaks are widely spaced. As T_2 is increasing, the linewidth of the absorption peak b becomes wider because of the increased value of γ_b (Fig. 4(c)). But the larger spacing of the absorption peaks can still give rise to the wide width of two transparency windows. In this situation, the steep dispersion within the transparency windows is not possible (Fig. 2(b) and (c)).

With increasing value of ω_{23}, the eigen energie λ_b is increased, while the eigen energie λ_a and λ_c are nearly unchanged (Fig. 4(b)). So the two absorption peaks a and b become closer, while the two absorption peaks b and c become farther. On the other hand, form Fig. 4(d), with increasing value of ω_{23}, the decay rate γ_b is increased dramatically, while the decay rate γ_a is increased a little bit. As a result, the linewidth of the absorption peak b becomes much larger. Therefore, the closer spaced absorption peaks a and b, and together the larger linewidth of the absorption peak b give rise to the narrower transparency window between peak a and peak b. And within the narrower transparency window, the steep dispersion profile of the probe field can be obtained (Fig. 2(d) and (e)).

So it can be concluded that the intensity of the tunneling coupling T_2 and the energy splitting ω_{23} of the TQDs can modify the position and the linewidth of the absorption peaks, which are responsible for the controlling of the narrow transparency windows. And within the narrow transparency windows, steep dispersion can be obtained.

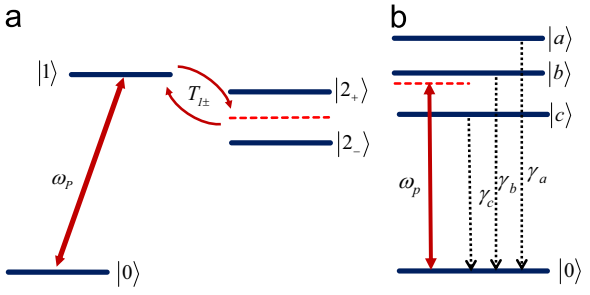

Fig. 3. (a) Dressed state under the coupling of the tunneling T_2. (b) Dressed state under the coupling of the tunneling T_1 and T_2.

4. Transmission spectrum of TDQs

In this part we embed the TQDs sample in a ring cavity, as shown in Fig. 5. We consider the optical cavity of length L with TQDs sample of length l. Then the cavity transmission can be

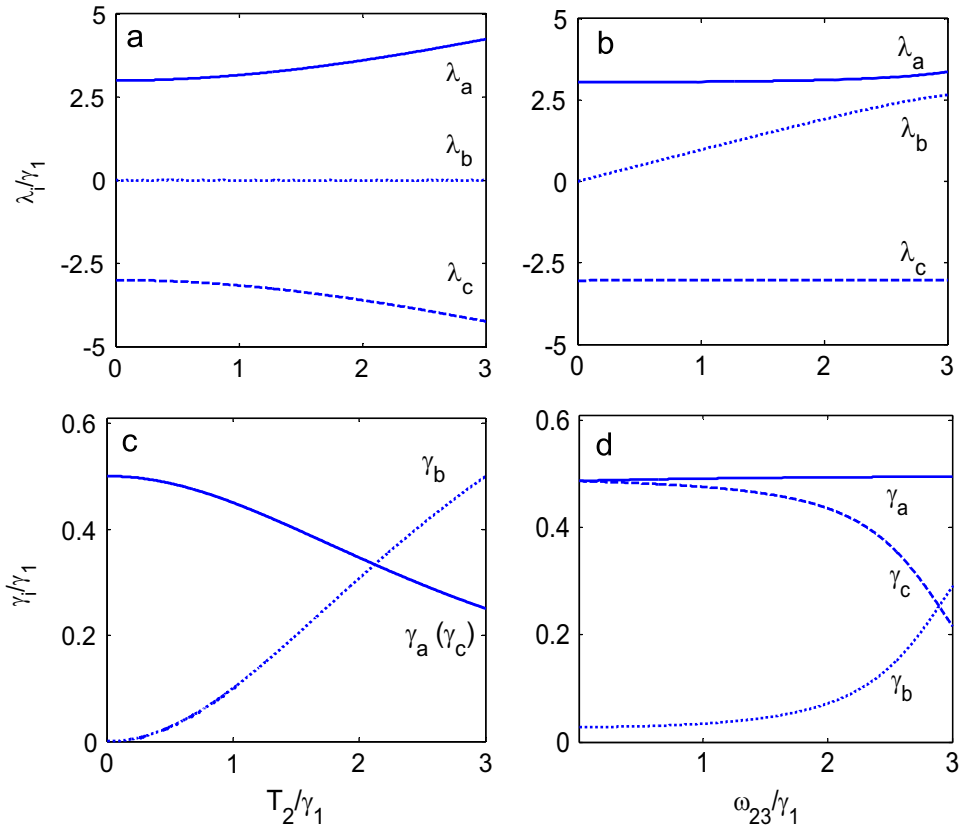

Fig. 4. (a) The eigen energies of the dressed state $\lambda_i(i=a,b,c)$, and (c) the decay rates $\gamma_i(i=a,b,c)$ as a function of T_2. (b) The eigen energies of the dressed state $\lambda_i(i=a,b,c)$, and (d) the decay rates $\gamma_i(i=a,b,c)$ as a function of ω_{23}.

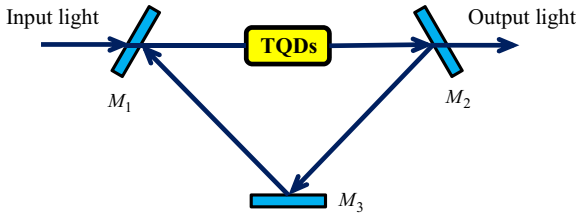

Fig. 5. The schematic of a cavity-TQDs system.

expressed as [3]

$$S(\omega)=\frac{t^2}{1+r^2\kappa^2-2r\kappa\ \cos\ [\Phi(\omega)]}, \tag{9}$$

here t and r denote the transmissivity and the reflectivity of both the input and the output mirrors with $r^2+t^2=1$. For simplicity, we assume that mirror 3 has 100% reflectivity. And $\Phi(\omega)=\frac{\omega}{c}(L+l\chi')$ is the total phase shift, which is contributed by the real part (χ') of the susceptibility of the TQDs. And $\kappa=\exp(-\frac{\omega}{c}l\chi'')$ is the medium absorption per round trip, which is caused by the imaginary part (χ'') of the susceptibility of the TQDs, leading to the attenuation of the amplification of the probe field.

On inspection of the round-trip phase shift, the pulling equation representing the resonance frequency of the combined cavity and medium system is [3]

$$\omega_r=\frac{1}{1+\eta}\omega_c+\frac{\eta}{1+\eta}\omega_p, \tag{10a}$$

$$\eta=\omega_p\frac{l}{2L}\frac{\partial\chi'}{\partial\omega_p}. \tag{10b}$$

Here η defines a frequency-locking or stabilization coefficient, which is relative to the dispersion of the system. Eq. (10) indicates that ω_r is contributed by two factors, one is the resonance frequency of the empty cavity ω_c, with $\omega_c=mc/L$ (for integer m), and the other is the probe transition frequency of TQDs. When EIT is induced in TQDs medium, the probe transition frequency ω_p is close to ω_{10}. Therefore the medium around transparency window will pull the resonance frequency ω_r to its respective EIT frequency.

Use the same methods in Ref. [3], the width of cavity resonances $\delta\omega$ changed by the intracavity medium is

$$\delta\omega=\frac{1-r\kappa}{\sqrt{\kappa}(1-r)}\frac{1}{1-\eta}\delta\omega_c, \tag{11}$$

where $\delta\omega_c$ is the empty-cavity linewidth. And $(1-r\kappa)/\sqrt{\kappa}(1-r)$ describes an enhancement of the effective cavity and medium width due to additional losses, while $1/(1-\eta)$ describes the reduction due to the linear dispersion. When EIT is induced, the absorption can be negligible ($\chi''\to 0$), whereas the dispersion is large, then Eq. (11) can be simplified as

$$\delta\omega=\frac{1}{1-\eta}\delta\omega_c. \tag{12}$$

Eq. (12) indicates that the steep dispersion will result in substantial linewidth narrowing of the transmission spectrum closer to the transparency windows.

According to Eq. (9), we plot the numerical simulation of the cavity transmission spectrum in Fig. 6 with the same parameters used in Fig. 2. First we consider the case only with the tunneling T_1. Thus the system is similar to DQDs, and single dark resonance is established. Therefore one can obtain one broad transmission peak locating at the position of the transparency window, as

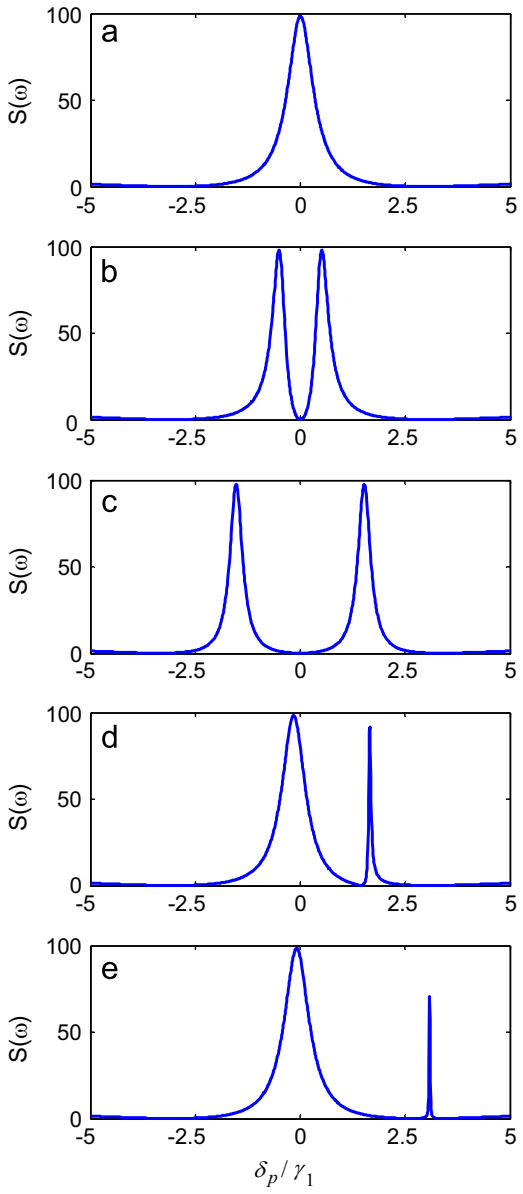

Fig. 6. The cavity transmission spectrum as a function of δ_p. The parameters are $r=0.98$, $r^2+t^2=1$, $L=20$ cm and $N\sigma_{10}l=0.5$. And other parameters refer to Fig. 2.

shown in Fig. 6(a). The dispersion shown in Fig. 2(a) is not large, which is responsible for the broad linewidth of the transmission peak. Next we apply both tunneling T_1 and T_2. In this case, one transmission peak turns into two transmission peaks because that double dark resonances are induced by the two tunneling couplings (Fig. 6(b)–(e). For $\omega_{12}=\omega_{23}=0$, the transmission spectrum in Fig. 6(b) and (c) are symmetrical and the linewidth narrowing of the transmission peaks is not obvious, because that the dispersion for two tunneling couplings dose not change much compared with the one for only one tunneling coupling. And with the increased value of tunneling T_2, the two transmission peaks become farther away from each other, but keep the linewidth nearly unchanged.

Next we show the case for $\omega_{23}\neq 0$ in Fig. 6(d) and (e), and find that an extranarrow transmission peak can be obtained. The extranarrow transmission peak is because of the much steeper slope of the dispersion, which is within the extranarrow transparency window in Fig. 2(d) and (e). With the increasing value of ω_{23}, the position of the narrowed transmission peak is moving to the red frequency side, and the linewidth of the transmission peak is becoming much narrower. From Fig. 6(b)–(e), the conclusion can be made that ω_{23} can not only modify the position of the transmission peak, but also narrow the linewidth of it. The narorowing of the transmission peak is due to the steep dispersion, which is resulted from the narrow transparency window.

5. Conclusions

In conclusion, we have proposed a scheme for obtaining a tunable ultranarrow cavity transmission controlled by tunneling in TQDs system. In such system, two transparency windows can be obtained, which is due to the double dark resonances induced by two tunneling couplings between the dots. By proper tuning the tunneling and the energy splitting, the transparency window can be made very narrow, and within the narrow transparency window steep dispersion can be acquired. Furthermore, when the sample is embedded in a ring cavity, ultranarrow transmission peak can be obtained compared with that of DQDs. And the linewidth and the position of this ultranarrow transmission peak can be controlled by adjusting the energy splitting. Such cavity-linewidth narrowing is due to the high dispersion and reduced absorption produced by the tunneling.

Acknowledgments

This work is supported by the financial support from the National Basic Research Program of China (Grant no. 2013CB933300), the National Natural Science Foundation of China (Grant no. 11304308 and 61176046), Jilin Provincial Natural Science Foundation (Grant no. 20140101203JC), and the Hundred Talents Program of Chinese Academy of Sciences.

References

[1] S.E. Harris, Phys. Today 52 (1997) 36.
[2] M. Fleischhauer, A. Imamoglu, J.P. Marangos, Rev. Mod. Phys. 77 (2005) 633.
[3] M.D. Lukin, M. Fleischhauer, M.O. Scully, V.L. Velichansky, Opt. Lett. 23 (1998) 295.
[4] H. Wang, D.J. Goorskey, W.H. Burkett, M. Xiao, Opt. Lett. 25 (2000) 1732.
[5] G. Hernandez, J.P. Zhang, Y.F. Zhu, Phys. Rev. A 76 (2007) 053814.
[6] H. Wu, J. Gea-Banacloche, M. Xiao, Phys. Rev. Lett. 100 (2008) 173602.
[7] M.D. Lukin, S.F. Yelin, M. Fleischhauer, M.O. Scully, Phys. Rev. A 60 (1999) 3225.
[8] Y.C. Chen, Y.A. Liao, H.Y. Chiu, J.J. Su, I.A. Yu, Phys. Rev. A 64 (2001) 053806.
[9] S.F. Yelin, V.A. Sautenkov, M.M. Kash, G.R. Welch, M.D. Lukin, Phys. Rev. A 68 (2003) 063801.
[10] Y.P. Niu, S.Q. Gong, R.X. Li, Z.Z. Xu, X.Y. Liang, Opt. Lett. 30 (2005) 3371.
[11] R.G. Wan, J. Kou, L. Jiang, Y. Jiang, J.Y. Gao, J. Opt. Soc. Am. B 28 (2011) 622.
[12] Z.P. Wang, B.L Yu, J. Lumin. 132 (2012) 2452.
[13] Q.H. Xie, A. Madhukar, P. Chen, N.P. Kobayashi, Phys. Rev. Lett. 75 (1995) 2542.
[14] G.J. Beirne, C. Hermannstadter, L. Wang, A. Rastelli, O.G. Schmidt, P. Michler, Phys. Rev. Lett. 96 (2006) 137401.
[15] E.A. Stinaff, M. Scheibner, A.S. Bracker, I.V. Ponomarev, V.L. Korenev, M.E Ware, M.F. Doty, T.L. Reinecke, D. Gammon, Science 311 (2006) (2006) 636.
[16] D. Kim, S.G. Carter, A. Greilich, A.S. Bracker, D. Gammon, Nat. Phys. 7 (2010) 223.
[17] A. Boyer de la Giroday, N. Sköld, R.M. Stevenson, I. Farrer, D.A. Ritchie, A.J. Shields, Phys. Rev. Lett. 106 (2011) 216802.
[18] K.M. Weiss, J.M. Elzerman, Y.L. Delley, J. Miguel-Sanchez, A. Imamoğlu, Phys. Rev. Lett. 109 (2012) 107401.
[19] C.H. Yuan, K.D. Zhu, Appl. Phys. Lett. 89 (2006) 052115.
[20] H.S. Borges, L. Sanz, J.M. Villas-Bôas, O.O. DinizNeto, A.M. Alcalde, Phys. Rev. B 85 (2012) 115425.
[21] S. Michael, W.W. Chow, H.C. Schneider, Phys. Rev. B 88 (2013) 125305.
[22] X.Y. Lü, J. Wu, L.L. Zheng, Z.M. Zhan, Phys. Rev. A 83 (2011) 042302.
[23] M.T. Cheng, X.S. Ma, Y.Q. Luo, P.Z. Wang, G.X. Zhao, Appl. Phys. Lett. 99 (2011) 223509.
[24] A.S. Zheng, Y.J. Cheng, J.B. Liu, J. Opt. Soc. Am. B 30 (2013) 3168.
[25] S.P. Liu, R. Yu, J.H. Li, Y. Wu, J. Appl. Phys. 115 (2014) 134312.
[26] J. Li, R. Yu, J. Liu, P. Huang, X. Yang, Physica E 41 (2008) 70.
[27] Z.P. Wang, S.L. Zhen, X.Q. Wu, J. Zhu, Z.G. Cao, B.L. Yu, Opt. Commun. 304 (2011) 7.
[28] E. Voutsinas, A.F. Terzis, E. Paspalakis, Phys. Lett. A 378 (2014) 219.
[29] Y.D. Peng, Y.P. Niu, N. Cui, S.Q. Gong, Opt. Commun. 284 (2011) 824.

[30] S.C. Tian, C.Z. Tong, C.L. Wang, L.J. Wang, H. Wu, E.B. Xing, Y.Q. Ning, L.J. Wang, Opt. Commun. 312 (2014) 296.
[31] C.Y. Hsieh, Y.P. Shim, M. Korkusinski, P. Hawrylak, Rep. Prog. Phys. 75 (2012) 114501.
[32] Q.H. Xie, A. Madhukar, P. Chen, N.P. Kobayashi, Phys. Rev. Lett. 75 (1995) 2542.
[33] G. Rainò, A. Salhi, V. Tasco, M. De Vittorio, A. Passaseo, R. Cingolani, M. De Giorgi, E. Luna, A. Trampert, J. Appl. Phys. 103 (2008) 096107.
[34] R. Songmuang, S. Kiravittaya, O.G. Schmidt, Appl. Phys. Lett. 82 (2003) 2892.
[35] R. Yu, J.H. Li, C.L. Ding, X.X. Yang, Phys. Lett. A 375 (2011) 2738.
[36] S.C. Tian, C.Z. Tong, C.L. Wang, Y.Q. Ning, J. Lumin. 153 (2014) 169.
[37] S.C. Tian, R.G. Gang, C.Z. Tong, Y.Q. Ning, L. Qin, Y. Liu, J. Opt. Soc. Am. B 31 (2014) 1436.
[38] J.T. Sheng, X.H. Yang, U. Khadka, M. Xiao, Opt. Express 19 (2011) 17059.
[39] Y.H. Wang, J.P. Zhang, Y.F. Zhu, Phys. Rev. A 85 (2012) 013814.
[40] K. Ying, Y.P. Niu, D.J. Chen, H.W. Cai, R.H. Qu, S.Q. Gong, J.Opt. Soc. Am. B 31 (2014) 144.
[41] G.S. Agarwal, Quantum Optics, Springer-Verlag, Berlin, 1974.
[42] S.M. Barnett, P.M. Radmore, Methods in Theoretical Quantum Optics, Oxford University Press, Oxford, 1997.
[43] J. Kim, S.L. Chuang, P.C. Ku, C.J. Chang-Hasnain, J. Phys.: Condens. Matter 16 (2004) S3727.
[44] S.E. Harris, Y. Yamamoto, Phys. Rev. Lett. 81 (1998) 3611.
[45] J.H. Wu, J.Y. Gao, J.H. Xu, L. Silvestri, M. Artoni, G.C. La Rocca, F. Bassani, Phys. Rev. Lett. 95 (2005) 057401.
[46] N.H. Bonadeo, J. Erland, D. Gammon, D. Park, D.S. Katzer, D.G. Steel, Science 282 (1998) 1473.
[47] H. Kamada, H. Gotoh, J. Temmyo, T. Takagahara, H. Ando, Phys. Rev. Lett. 87 (2001) 246401.
[48] A. Tackeuchi, T. Kuroda, K. Mase, Phys. Lett. B 62 (2000) 1568.
[49] P. Chen, C. Piermarocchi, L.J. Sham, Phys. Rev. Lett. 87 (2001) 067401.
[50] V. Negoita, D.W. Snoke, K. Eberl, Phys. Lett. B 60 (1999) 2661.
[51] P. Borri, W. Langbein, U Woggon, M. Schwab, M. Bayer, S. Fafard, Z. Wasilewski, P. Hawrylak, Phys. Rev. Lett. 91 (2003) 267401.
[52] C. Bardot, M. Schwab, M. Bayer, S. Fafard, Z. Wasilewski, P. Hawrylak, Phys. Lett. B 72 (2005) 035314.
[53] L.V. Butov, A. Zrenner, G. Abstreiter, G. Bohm, G Weimann, Phys. Rev. Lett. 73 (1994) 304.